



**HAL**  
open science

## Overexpression and role of the ATPase and putative DNA helicase RuvB-like 2 in human hepatocellular carcinoma.

Benoît Rousseau, Ludovic Ménard, Valérie Haurie, Danièle Taras, Jean-Frédéric Blanc, François Moreau-Gaudry, Philippe Metzler, Michel Hugues, Sandrine Boyault, Sylvie Lemièrre, et al.

► **To cite this version:**

Benoît Rousseau, Ludovic Ménard, Valérie Haurie, Danièle Taras, Jean-Frédéric Blanc, et al.. Overexpression and role of the ATPase and putative DNA helicase RuvB-like 2 in human hepatocellular carcinoma.. *Hepatology*, 2007, 46 (4), pp.1108-18. 10.1002/hep.21770 . inserm-00173425

**HAL Id: inserm-00173425**

**<https://inserm.hal.science/inserm-00173425>**

Submitted on 24 Sep 2007

**HAL** is a multi-disciplinary open access archive for the deposit and dissemination of scientific research documents, whether they are published or not. The documents may come from teaching and research institutions in France or abroad, or from public or private research centers.

L'archive ouverte pluridisciplinaire **HAL**, est destinée au dépôt et à la diffusion de documents scientifiques de niveau recherche, publiés ou non, émanant des établissements d'enseignement et de recherche français ou étrangers, des laboratoires publics ou privés.

## **Overexpression and role of the ATPase and putative DNA helicase RuvB-like 2 in human hepatocellular carcinoma**

Benoît Rousseau<sup>1,\*</sup>, Ludovic Ménard<sup>1,\*</sup>, Valérie Haurie<sup>1</sup>, Danièle Taras<sup>1</sup>, Jean-Frédéric Blanc<sup>1,2</sup>, François Moreau-Gaudry<sup>3</sup>, Philippe Metzler<sup>1</sup>, Michel Hugues<sup>1</sup>, Sandrine Boyault<sup>4</sup>, Sylvie Lemièrè<sup>5</sup>, Xavier Cannon<sup>5</sup>, Pierre Costet<sup>6</sup>, Michael Cole<sup>7</sup>, Charles Balabaud<sup>1,2</sup>, Paulette Bioulac-Sage<sup>1,2</sup>, Jessica Zucman-Rossi<sup>4</sup>, Jean Rosenbaum<sup>1</sup>

<sup>1</sup>INSERM, U889, Bordeaux, F-33076 France; Université Victor Segalen Bordeaux 2, IFR 66, Bordeaux, F-33076 France.

<sup>2</sup>CHU, Groupement des Spécialités Digestives, Bordeaux, F-33076 France.

<sup>3</sup>INSERM, E217, Bordeaux, F-33076 France; Université Victor Segalen Bordeaux 2, IFR 66, Bordeaux, F-33076 France.

<sup>4</sup>INSERM, U674, CEPH, IUH, Paris, F-75010 France.

<sup>5</sup>INSERM, E113, Talence, F-33405 France; Université Bordeaux 1, IFR 66, Talence, F-33405 France.

<sup>6</sup>Université Victor Segalen Bordeaux 2, Animalerie spécialisée, Bordeaux, F-33076 France.

<sup>7</sup>Dartmouth Medical School, Department of Pharmacology and of Genetics, Lebanon, NH 03756 USA.

\* BR and LM contributed equally to this work

Keywords : beta-catenin, apoptosis, RNA interference, repton, TIP48

## Footnote page

### Corresponding author :

Jean ROSENBAUM

GRAF, INSERM U889, Université Victor Segalen Bordeaux 2, 146 rue Léo Saignat, 33076 Bordeaux, France. Tel : +33 5 57 57 15 94; Fax : +33 5 56 51 40 77; mail : [jean.rosenbaum@gref.u-bordeaux2.fr](mailto:jean.rosenbaum@gref.u-bordeaux2.fr)

List of abbreviations : HCC : hepatocellular carcinoma; PCR: polymerase chain reaction; RT: reverse transcription; MTT : 3-(4,5-dimethylthiazol-2-yl)-2,5-diphenyltetrazolium bromide.

Grant support : This work was funded by grants from Association pour la Recherche sur le Cancer, Agence Nationale pour la Recherche sur le SIDA et les Hépatites, Société Nationale Française de Gastroentérologie and Conseil Régional d'Aquitaine. PM was the recipient of a fellowship from Fondation pour la Recherche Médicale.

## Abstract

Using a proteomic analysis of human hepatocellular carcinoma (HCC), we identified the overexpression in 4 tumors of RUVBL2, an ATPase and putative DNA helicase, known to interact with  $\beta$ -catenin and c-myc. RUVBL2 expression was further analyzed in tumors with quantitative RT-PCR and immunohistochemistry; in addition, RUVBL2 expression in HuH7 cell line was silenced by siRNA or increased using a lentiviral vector. RUVBL2 mRNA overexpression was confirmed in 72 out of 96 HCC cases and it was associated with poorly differentiated tumors ( $p=0.02$ ) and to a poor prognosis ( $p=0.02$ ), but not with  $\beta$ -catenin mutations or c-myc levels. Whereas RUVBL2 was strictly nuclear in normal hepatocytes, tumoral hepatocytes exhibited an additional cytoplasmic staining. There was no mutation in the coding sequence of RUVBL2 in 10 sequenced cases. Silencing RUVBL2 in HuH7 HCC cells reduced cell growth ( $p < 0.001$ ) and increased apoptosis as shown by DNA fragmentation ( $p < 0.001$ ) and caspase 3 activity ( $p < 0.005$ ). This was associated with an increased expression of several pro-apoptotic genes, and with an increased conformational activation of Bak-1 **and Bax**. On the other hand, HuH7 cells with overexpression of RUVBL2 grew better in soft agar ( $p < 0.03$ ), had an increased resistance to C2 ceramide-induced apoptosis ( $p < 0.001$ ) and gave rise to significantly larger tumors when injected to immunodeficient Rag2/ $\gamma$ c mice ( $p = 0.016$ ). In conclusion, RUVBL2 is overexpressed in a large majority of HCC. RUVBL2 overexpression enhances tumorigenicity and RUVBL2 is required for tumor cell viability. These results argue for a major role of RUVBL2 in liver carcinogenesis.

Hepatocellular carcinoma (HCC) is the most frequent primary liver cancer. Despite the discovery of several carcinogenetic pathways, the mechanisms of liver carcinogenesis are still unclear (1). It is also apparent that the underlying mechanisms may be different according to the etiology of the HCC (2, 3). Due to its high incidence in occidental countries, hepatitis C is responsible for a strong increase in HCC incidence. As several other groups (4, 5), we have recently applied proteomics technology to discover new markers or targets in HCV-related HCC. This was done using 2D-electrophoresis and mass spectrometry and led to the discovery of many regulated proteins (6) including the recently uncovered protein RUVBL2, also known as TIP49b (7), TIP48 (8), Reptin52 (9), Rvb2 (10), TAP54 $\beta$  (11), ECP-51 (12) and TIH2p (13). RUVBL2 contains the Walker A and Walker B motifs which are found in proteins that bind and hydrolyze ATP (14). RUVBL2 also has limited homology to the bacterial RuvB ATP-dependent DNA helicase. Human RUVBL2 has indeed been shown to have ATPase activity (7, 11) whereas its DNA helicase activity has been disputed (7, 11). RUVBL2 is found in several nuclear high molecular weight chromatin-remodeling complexes (10, 11). Recently, it was found that RUVBL2 was able to interact with  $\beta$ -catenin resulting in altered TCF/LEF-mediated transcription (9, 15). RUVBL2 also interacts with a domain of c-myc required for oncogenic transformation (8) and its expression is controlled by c-myc itself (8, 16). Given that  $\beta$ -catenin and c-myc are two key actors of liver carcinogenesis, our study was designed to assess the role of RUVBL2 in liver carcinogenesis.

## **Experimental procedures**

### Liver samples

Samples came from resected or explanted livers with HCC of patients treated in Bordeaux from 1992 to 2005. Fragments of fresh tumoral and non-tumoral liver tissues (taken at a

distance of at least 2 cm from the tumor) were immediately snap-frozen in liquid nitrogen and stored at -80°C. DNA and RNA were extracted as described (17). The proteomic study included 4 male patients (mean age 77, range 72-82) with HCC developed on chronic viral hepatitis C (stage F3 for 3 patients and F2 for one patient, according to Metavir classification (18)). In addition, HCC samples from 96 patients related to various etiologies were used for quantitative RT-PCR analysis and immunohistochemistry. The main clinical and pathological characteristics are indicated in Table 1. Six normal liver samples taken at distance from benign liver tumors were used as controls in quantitative RT-PCR and immunohistochemistry. Survival analysis included 45 patients treated with a complete tumor resection before 2002; patients treated with liver transplantation, incomplete resection, or deceased in the post-operative period were excluded.

### Proteomic analysis

Four tumoral samples were compared to matched non-tumor samples using 2D electrophoresis as previously described in detail (6).

### Real-time RT-PCR

Liver samples. One  $\mu\text{g}$  of total RNA was reverse transcribed using the High capacity Archive kit and random hexamers (Applied Biosystems) and 5  $\mu\text{l}$  of cDNA corresponding to 10 ng of reverse transcribed RNA were analyzed by TaqMan PCR analysis, in duplicate, using the ABI PRISM<sup>®</sup> 7900HT System (Applied Biosystems). Pre-developed sequence detection reagents specific for human *RUVBL2* gene (Applied Biosystems) were used as described (17) using the  $2^{-\Delta\Delta\text{CT}}$  method (19). Briefly, gene expression results were first normalized to internal control ribosomal 18S. Then, results in HCC samples were expressed as a ratio relatively to the mean expression level in non-tumor samples. We also measured the mRNA level of expression for

c-myc, *GLUL* (encoding glutamine synthase) and *GPR49* (encoding an orphan nuclear receptor), two well known  $\beta$ -catenin target genes, as previously described (20). Finally, mutations in the *CTNGB1* gene coding for  $\beta$ -catenin were searched as described (2).

Cellular samples. Total RNA was extracted using Trizol<sup>®</sup> reagent (Invitrogen). One  $\mu$ g of total RNA was reverse transcribed using the Superscript<sup>™</sup> II reverse transcriptase (Invitrogen) and random hexamers (Roche). Five  $\mu$ l of cDNA corresponding to 5 ng of reverse transcribed RNA were analyzed by SYBR Green PCR analysis using the Mx4000<sup>®</sup> Multiplex Quantitative PCR System (Stratagene). PCR mixes were made such that each 25  $\mu$ l reaction contained 12.5  $\mu$ l of iQ Sybr Green Supermix (BioRad), 5  $\mu$ l of diluted cDNA template and 0.3  $\mu$ M sense and antisense gene primers. Primer sequences are shown in supplementary Table 1. The reactions were incubated at 95°C for 3 min, followed by 40 cycles of 95°C for 15s and 65° for 15s. Data analysis was performed using the Mx4000 software version 4.2 (Stratagene). Gene expression results were first normalized to internal control RLP0. Relative levels of expression were quantified by calculating  $2^{-\Delta\Delta Ct}$ . Results were expressed as a ratio relatively to the expression level in non-transfected cells.

### Immunohistochemistry

Twenty samples of HCC and their corresponding non tumoral liver were evaluated by immunohistochemistry, together with 6 normal liver samples. Formalin-fixed, paraffin-embedded sections were used. Following dewaxing and dehydration, sections were submitted to antigen retrieval using a steam cooker in citrate buffer 0.01 M pH 7 for 10 min, then permeabilized with methanol for 1h. The immunostaining procedure was carried out in an Autostainer (Dako). Endogenous peroxidase was inhibited with 3% H<sub>2</sub>O<sub>2</sub> in methanol and sections were treated with 2N HCl for 30 min at 37°C. Non specific sites were saturated with 3% BSA and sections were incubated with a mouse monoclonal anti-RUVBL2 antibody (BD

Biosciences) diluted 1:50. After washing, the signal was amplified with the Envision™ reagent coupled to horseradish peroxidase. The staining was revealed with diaminobenzidine.

### Construction of a cell line with overexpression of RUVBL2

We used the human hepatocellular carcinoma cell line HuH7. A Flag-tagged RUVBL2 cDNA was placed under the control of the MND promoter as follows. The MND promoter (Myeloproliferative sarcoma virus enhancer, Negative control region deleted, dl587rev primer-binding site substituted) was removed from a lentiviral construct (21). The pRRLSIN.cPPT-PGK-WPRE, a self-inactivating human immunodeficiency virus type-1 (HIV-1)-based vector containing the central polypurine and termination tract (cPPT) and the woodchuck hepatitis virus posttranscriptional regulatory element (WPRE), was provided by D. Trono (Geneva, Switzerland). In short, we replaced the PGK promoter with the MND promoter. Then, a cDNA coding human RUVBL2 with a N-terminal FLAG tag (8) was cloned downstream of the MND promoter, leading to the TMRepW vector. As a control, we constructed the TMEW vector by cloning the EGFP cDNA instead of the RUVBL2 sequence. VSV-G pseudotyped lentivectors were produced by triple-transient transfection of 293T cells (22). Titers were determined by transducing 293T cells with serial dilution of lentiviral supernatant and analyzed for EGFP expression 5 days later. **Finally, HuH7 cells** were transduced with lentiviral vectors at a multiplicity of infection of 20 and/or 10 in DMEM 10% FCS medium with 8µg/mL protamine sulfate (Sigma, St Louis, MI). Infection efficiency was checked by testing for EGFP expression by flow cytometry.

### Transient transfection of siRNA

We used siRNAs targeting 2 separate sequences from RUVBL2 mRNA. The sequence 5'-GATGATTGAGTCCCTGACCAA-3' corresponds to nucleotides 552-572 from the reference



sequence (gi:9367026) and will be referred to as siR1, while the sequence 5'-GAAGATGTGGAGATGAGTGAG-3' corresponds to nucleotides 1153-1173 and will be referred to as siR2. As a control, we used a scrambled sequence from siR2, 5'-GGATGTAAGTGGGAAAGTGGA-3'. The corresponding oligonucleotides were bought from Eurogentec (Searing, Belgium) as duplexes and were transfected into HuH7 cells with Lipofectamine (InVitrogen, Cergy Pontoise, France) at a concentration of 125 nM.

### Western blot

Cell extracts and tissue samples were prepared in RIPA buffer as described (23). Protein concentration was measured with a BioRad assay. Samples were analyzed by Western blot with either a rabbit polyclonal (8) or a mouse monoclonal antibody (BD Biosciences Pharmingen) to RUVBL2 (# 612482), or an anti-Flag M2 antibody (Sigma). Normalization was achieved by rehybridization with an anti-beta-actin antibody. Signals were acquired on a Macintosh computer using a Kodak Digital Science DC 120 digital camera and quantified using the NIH Image software.

### Cell proliferation

Proliferation of cells transfected with siRNAs was assessed by counting adherent cells at varying times using a Coulter counter (Beckman Coulter) in duplicate wells.

DNA synthesis was measured by quantifying the incorporation of bromodeoxyuridine (BrdU). Briefly, cells were incubated for 2 h with 15 mM BrdU. They were fixed with methanol, treated with 2N HCl and incubated with a rat anti-BrdU antibody (Serotec) followed by an Alexa fluor 488 labeled secondary antibody (InVitrogen Molecular Probes). Nuclear DNA was stained with DAPI. BrdU-positive cells were counted under a fluorescence microscope in at least 15 non overlapping fields and results were expressed as a percentage of total cells.

We also measured the percentage of cells expressing the proliferation antigen Ki67 (24). Briefly, cells were fixed with 0.4 % paraformaldehyde, permeabilized with 0.02 % saponin, then incubated with a FITC-labeled Ki67 antibody (Dako) and analyzed by flow cytometry.

Anchorage-independent growth was assayed as follows. Flag-RUVBL2 expressing cells or control cells (10,000) were suspended in DMEM containing 10 % FCS and 0.2% agar (overlay) on top of an agar underlay (DMEM/10% FCS/0.5% agar) in a 60 mm diameter dish. Cells were fed twice a week with 2 ml of overlay medium, and the area of colonies was measured after 2 weeks using Image J software (<http://rsb.info.nih.gov/ij/>). Thirty different fields (5X) were scored. The experiments were done in triplicate.

#### Assay for cell viability

Cells were seeded at a density of 6,000/well in 96w plates. After 7h, they were treated with the indicated agonists for 17h. Cell viability was assessed by incubating with DMEM containing 1 mg/mL of 3-(4,5-dimethylthiazol-2-yl)-2,5-diphenyltetrazolium bromide (MTT) during 2 hours at 37°C as described (25). The linearity of the assay over the range of cell densities was checked in preliminary experiments.

#### Apoptosis

Cells were fixed using PFA 4% in PBS at 4°C during 10 min, then permeabilized with 0.5 % Triton X-100. They were stained with DAPI (Sigma, 0.5 µg/ml) together with a rabbit anti-human active caspase 3 antibody (R&D systems, 0.25 µg/ml). After washing, cells were incubated with goat anti-rabbit Alexa 488 (Molecular Probes) and examined under a Zeiss Axioplan microscope.

The extent of DNA fragmentation was quantified with flow cytometry as described (26). Briefly, trypsinized cells were resuspended in 0.1% sodium citrate containing 0.1% Triton X-

100, 50 µg/ml propidium iodide and 100 µg/ml RNase. Cell DNA content was measured using a FACScalibur (BD Biosciences, San Jose, CA, USA).

We also quantified caspase 3 activity using a colorimetric kit from Chemicon (Temecula, California), according to instructions from the supplier. Briefly, cleared cell extracts were incubated with the caspase 3 substrate and optical density was read at 405 nm in a Dynatech microplate reader (MTX Lab Systems, Inc., Vienna, VA).

Finally, we assessed Bak-1 and Bax activation using antibodies (Bak- 1 : AM03, Calbiochem, VWR International, Fontenay-sous-Bois, France ; Bax : 6A7 BD Pharmingen, Le Pont de Claix, France) that recognizes the N-terminus of the proteins made accessible following the conformational changes upon activation. This was done using flow cytometry as described by others (27, 28).

### Xenografts

12 weeks-old Rag2/γc mice (gift of J Di Santo (29)) were housed in germ-free conditions. The study was performed in accordance with the European Community Standards on the Care and Use of laboratory Animals. Mice were injected subcutaneously with  $2 \times 10^6$  cells in the flank. Tumor size was monitored with calipers. Tumor volume was estimated as  $(D^2 \times d)/2$ , where D is the large diameter and d is the small diameter of the tumor. At the end of the experiment, tumors were harvested and a part was snap-frozen in liquid nitrogen.

### Statistical analysis

Differences between means were assessed using the Mann-Whitney test. When comparing multiple means, we used an analysis of variance. A p value less than 0.05 was considered significant. Correlation between mRNA level of expression and qualitative variables were calculated using the non-parametric Kruskal-Wallis test with STATA software (Stata

corporation, Texas). Age of patients and diameter of tumors were partitioned using median. Survival analyses were performed using Cox model to fit maximum-likelihood proportional hazards models using STATA software.

## Results

### RUVBL2 expression in HCC

Proteome analysis was performed using 2DE gel electrophoresis comparing 4 HCC related to HCV infection with their matched non-tumor tissues. One of the 850 protein spots detected was increased in all 4 cases of HCC with a mean tumor/non tumor ratio of 4.1 (range 2.8-6.9) (Fig. 1A). It was identified as RUVBL2, based on the detection of two peptides (GLGLDDALEPR and LLIVSTTPYSEK) and detailed MS/MS analysis as previously described (6). Overexpression of RUVBL2 was confirmed by western blot in these 4 cases (Fig. 1B).

The cellular localization of RUVBL2 was assessed by immunohistochemistry in 20 samples of HCC from various etiologies and in the corresponding non tumoral livers, as well as in 4 cases of histologically normal livers. In normal liver, RUVBL2 expression was found in a variable fraction of hepatocytes, where it was faint and restricted to the nucleus; in addition, RUVBL2 staining was intense in bile duct cells where it was found in the nucleus and cytoplasm, and was also observed in some lymphocytes, either sinusoidal or portal (Fig. 2A). The same staining pattern, in terms of distribution and intensity, was seen in all samples of peri-tumoral livers, whether cirrhotic or not (Fig. 2C and 2F). In sharp contrast, RUVBL2 was overexpressed in all analyzed HCC (Fig. 2C), where in addition it showed a definite cytoplasmic staining that varied from faint to intense (Fig. 2D-E); in addition, nuclear staining of tumor cells was in most cases stronger than that of peri-tumoral hepatocytes (Fig. 2D-E). It should be noted however that the staining pattern was often heterogeneous within a given

tumor (Fig. 2C). In order to search for detailed clinico-pathological correlations, we measured RUVBL2 mRNA expression in a larger series of 96 well-annotated HCC related to various risk factors. We first confirmed in this series the increased expression of RUVBL2 transcripts in 72/96 HCC, ranging from 1.5 to 6.6 when compared with non-tumor liver tissues that ranged from 0.42 to 1.5 ( $p= 0.002$ , Fig. 3A). RUVBL2 expression was significantly lower in HBV related HCC (Fig. 3B) whereas it was significantly higher in poorly differentiated tumors proportionally to the Edmondson grade (Fig. 3C). In contrast, the other clinical and pathological characteristics mentioned in Table 1 were not significantly associated to RUVBL2 expression level. Using a Cox model analysis without partition, we showed a significant relationship between a high level of RUVBL2 in tumors and shorter overall survival of patients following surgery ( $p= 0.02$ ; relative risk 1.4, standard error 0.2, CI 95% 1.05-1.85). In contrast, we did not find a difference of RUVBL2 expression in  $\beta$ -catenin-activated HCC when compared to CTNNB1 non-mutated HCC (Fig. 3D). Accordingly, in the 96 HCC samples, we did not observe any correlation between the expression level of RUVBL2 and of  $\beta$ -catenin target genes (GLUL and GPR49, data not shown). In addition, c-myc transcript levels were measured in a subset of 42 patients and no correlation was found with RUVBL2 levels ( $r^2 = 0.01$ ,  $p = 0.5$ , not shown).

Finally, the whole coding sequence of RUVBL2 was PCR-amplified in 10 HCC samples and no mutation leading to a change in amino-acid sequence was identified (not shown).

Thus, because RUVBL2 over-expression was found in the vast majority of HCC and was related to the aggressiveness of tumors, we explored the role of RUVBL2 in tumorigenesis by modulating its expression in the HCC cell line HuH7.

### Down-regulation of RUVBL2 expression reduced cell growth and increased apoptosis

Down-regulation of RUVBL2 expression was obtained using transient transfections of siRNA duplexes. Quantitative RT-PCR showed that as soon as 24 h after transfection, RUVBL2 transcripts were reduced to  $33.5 \pm 9.8\%$  with siR1 and  $29.5 \pm 14.4\%$  with siR2, as compared to  $104.4 \pm 15.4\%$  with the scrambled sequence ( $n = 6$ ,  $p = 0.02$ ). In addition, as shown on Fig. 4A, the two targeting siRNAs led to a large decrease in RUVBL2 protein expression that reached more than 90% with siR1 and close to 80% with siR2. In both cases, the decrease was stable for at least 6 days.

We next evaluated the effect of RUVBL2 down expression on cell growth. Following a slight reduction in cell **numbers** observed at Days 3-4 post-transfection with either scrambled or RUVBL2 siRNAs (siR1 and siR2), a marked and significant reduction **in cell numbers** was observed in siR1 and siR2 transfected cells until day 6 when compared with non transfected or scrambled transfected cells ( $p < 0.001$ , Fig 4B); the reduction was more drastic with siR1 than siR2. **This reduction was linked to a decreased cell proliferation as evidenced by the measure of BrdU incorporation : at Day 4 post-transfection, there was an average of  $37.0 \pm 1.5\%$  labeled cells with the scramble oligonucleotide, as compared to  $21.7 \pm 1.0\%$  with siR1. The mean decrease with siR1 was  $41.0 \pm 4.4\%$  ( $n = 3$ ,  $p < 0.04$ ). Similarly, the percentage of cells positive for Ki67 was significantly decreased by both siR1 and with siR2 (Fig. 4C).**

In parallel, we observed that down regulation of RUVBL2 expression was associated with a high number of cells floating in the supernatant **(not shown)**, suggesting that the cells may undergo apoptosis. This was confirmed by staining nuclear DNA with DAPI showing characteristic pictures of fragmented nuclei in RUVBL2 siRNA-transfected cells (Fig. 4E), as compared to scrambled (Fig. 4D). Simultaneous staining of the cells with an antibody specific for activated caspase 3 demonstrated that many cells transfected with RUVBL2 siRNAs showed an activation of this apoptotic pathway (compare Fig. 4G and 4F). DNA

fragmentation was quantified with flow cytometry that showed a significantly higher percentage of fragmented DNA at Day 6 post-transfection in cells transfected with siR1 or siR2 than in scrambled-transfected cells (ANOVA,  $p < 0.001$ ; Fig 4J). Similarly, quantification of caspase 3 activity with a colorimetric assay showed a significantly increased activity with both siR1 and siR2, as shown on Fig. 4K (ANOVA,  $p < 0.005$ ).

In order to gain insight into the mechanisms of apoptosis, we measured the activation of the pro-apoptotic Bcl-2 family members Bax and Bak-1. These 2 proteins undergo a conformational activation that can be evidenced using conformation-sensitive antibodies in flow cytometry. As shown on Fig. 5A-B, the number of cells showing activation of either Bax or Bak-1 was significantly increased upon down-regulation of RUVBL2. In addition, we also show a significantly increased expression of the transcripts of Bak-1 and of the other pro-apoptotic proteins Bad and Bid at Days 3 and 4 post-transfection of RUVBL2 siRNA, and of Bcl-xS at Day 4. There was also a trend towards an increase for Bax and PUMA, whereas no changes were seen for the anti-apoptotic gene Bcl-xL (Fig. 5C-D).

Up-regulation of RUVBL2 expression promotes *in vitro* anchorage-independent cell growth and *in vivo* tumorigenesis

Here, Flag-tagged RUVBL2 was overexpressed under the control of the MND promoter in a lentiviral vector. Flag-tagged RUVBL2 could be easily detected and discriminated from endogenous RUVBL2 on Western blots due to its slower gel mobility. The factor of overexpression of RUVBL2 protein, assessed by making the sum of the intensities of the endogenous and the Flag-tagged RUVBL2 bands, was of only 1.2 in 2 independent transductions. This was due at least in part to a decrease in endogenous RUVBL2 levels in Flag-RUVBL2-infected cells (Fig. 6A). Several preliminary experiments allowed us to check that Flag-tagged RUVBL2 behaved similarly as endogenous RUVBL2 : western blot of

nuclear and cytosolic extracts showed that both forms segregated alike in these 2 compartments; immunoprecipitation of Flag-tagged RUVBL2 pulled down expected partners (RUVBL1 and  $\beta$ -catenin (9)) indicating that the tagged protein was correctly incorporated into supra-molecular complexes (data not shown).

The growth rate on plastic of Flag-RUVBL2-expressing cells was compared to that of control EGFP-transfected cells. No differences in cell numbers were seen after 1, 2 or 3 days in serum concentrations ranging from 0.5 to 10% (data not shown). However, when anchorage-independent growth was measured in a soft agar assay, we found a large difference in the growth ability of Flag-RUVBL2-expressing cells, as shown by a significant increase in the surface of the colonies (Fig. 6B,  $p < 0.03$ , Kruskal-Wallis).

In subsequent experiments HuH7 cells were challenged with an apoptotic stimulus, C2 ceramide (30), and cell survival was assessed with the MTT assay. At every concentration of C2 ceramide tested, cells expressing Flag-RUVBL2 were slightly less susceptible to cell death than control cells. The difference was statistically significant except for the highest concentration of C2 ceramide when most cells were dead (Fig. 6C). Furthermore, when the extent of DNA fragmentation, as an evidence for apoptosis, was examined, cells expressing Flag-RUVBL2 exhibited a significant protection over a range of C2 ceramide concentrations, as compared with control cells (Fig. 6D). The fractional reduction in apoptosis as compared to control cells was  $27.2 \pm 6.0\%$ ,  $19.3 \pm 8.5\%$  and  $28.7 \pm 3.3\%$  at 20, 40 and 60  $\mu\text{M}$  C2 ceramide, respectively.

Finally, cells transduced with either EGFP or Flag-tagged RUVBL2 were injected to immunocompromised mice ( $n = 20$  in each group). Although there was no significant difference in the incidence of tumors in both groups (85.0 vs 94.7% in EGFP and RUVBL2 groups, respectively), animals injected with Flag-RUVBL2-expressing cells developed significantly larger tumors than control animals (Fig. 6E,  $p = 0.016$  by ANOVA). Similar



results were obtained in another experiment using cells from an independent transduction with the viral vectors. When at the end of the experiment, tumors from surviving animals were removed and analyzed by Western blot, the persistence of Flag-RUVBL2 expression was confirmed in every tumor in the Flag-RUVBL2 group by the detection of a doublet upon blotting with RUVBL2 antibody, and by the detection of the Flag epitope (Fig. 6F). This also showed the persistent decrease in endogenous RUVBL2.

## Discussion

Here, we show that RUVBL2 is up-regulated in a majority of HCCs. This over-expression is significantly associated with the differentiation grade of the tumors and RUVBL2 over-expression can be considered as a marker of poor prognosis. Moreover, our results strongly suggest that RUVBL2, a protein with no specific function yet ascribed in human, may play an essential role in liver carcinogenesis. To our knowledge, our findings are the first to report the deregulation of RUVBL2 expression in cancer. Our immunohistochemical data indicate that hepatocyte RUVBL2 expression appear increased in every HCC studied, although to a various extent. It is likely that tumor/non tumor ratios obtained with RT-PCR are artefactually low because of the high-level expression of RUVBL2 seen in the ductular proliferation of the non tumoral, cirrhotic livers (Fig. 2F).

Cells where RUVBL2 was down-regulated showed a decreased proliferation rate, concomitant with a strong induction of apoptosis, as evidenced by the occurrence of DNA fragmentation and increased caspase 3 activity. In addition to HuH7, we observed a similar phenotype in 2 other HCC cell lines, Hep3B and FOCUS (not shown). Thus, RUVBL2 deficiency leads to liver cancer cell growth arrest and to apoptosis. RUVBL2 was previously shown to be also required for growth and survival of yeast (7, 31, 32). Our data have shed some light on the mechanisms of apoptosis induced by RUVBL2 deficiency. We show that

RUVBL2 downregulation is associated with the increased conformational activation of the pro-apoptotic proteins Bak-1 and Bax. In quiescent cells, Bak-1 and Bax are maintained in an inactive state through interactions with the anti-apoptotic proteins Bcl-xL and Mcl-1 (33). Their activation leads to the permeabilization of the outer membrane of mitochondria, resulting in cytochrome c release and caspase activation. In addition to protein activation, we also found that Bak-1 and Bax transcripts were upregulated, together with those of Bid, a BH3-only protein involved in Bak-1 and Bax activation (34, 35), whereas interestingly, Bcl-xL levels did not increase. These changes were seen as early as Day 3, well before the occurrence of cell death, suggesting that they may play a causal role. We thus propose that apoptosis induced by RUVBL2 depletion is linked to the activation of pro-apoptotic Bcl-2 family members. Such a mechanism could be amplified because of the transcriptional upregulation of these proteins. Whether the related genes are direct targets of RUVBL2 remains to be determined.

We then transduced cells with a lentiviral construct driving the expression of Flag-RUVBL2. This led to only a modest increase in total expression of RUVBL2 which was not the consequence of a low level of transduction or of insufficient promoter activity, since RUVBL2 mRNA levels were  $7.5 \pm 2.2$ -fold higher in transduced cells as compared to control cells (not shown). The post-transcriptional regulation responsible for this is currently under study. Despite this modest 20% increase, Flag-RUVBL2 cells grew better in soft agar than control cells. Moreover, when Flag-RUVBL2 expressing cells were injected to immunocompromised mice, tumors grew eventually to a larger size. The mechanism for this effect remains to be evaluated in more depth, but may be partly related to a better ability of Flag-RUVBL2 expressing cells for survival in stressful conditions. We indeed found that Flag-RUVBL2 expressing cells were less susceptible to cell killing induced by the pro-apoptotic agent C2 ceramide. Although the protection was limited, it was in the range of 20-

30% at various concentrations of C2 ceramide, thus commensurate with the 20% overexpression of RUVBL2.

RUVBL2 is known to physically interact with  $\beta$ -catenin (9). Several publications have shown that RUVBL2 behaved as an antagonist of the transcriptional activity of the  $\beta$ -catenin-TCF/LEF complex (9, 15). Since  $\beta$ -catenin is considered an oncogene in HCC, these results appear counter-intuitive. However, recently, RUVBL2 was also found to be required for the repressing effect of  $\beta$ -catenin on the transcription of the anti-metastatic gene KAI-1 (36), that is frequently down-regulated in HCC (37). In our study of a large number of HCC samples, there were however no correlations between the level of expression of RUVBL2 and of  $\beta$ -catenin target genes. It is thus likely that additional mechanisms, independent of  $\beta$ -catenin, may also explain the oncogenic properties of RUVBL2. Indeed, RUVBL2 has been found in supra-molecular complexes that do not include  $\beta$ -catenin (11), and  $\beta$ -catenin-independent functions of RUVBL2 have already been identified (15). It is also noteworthy that RUVBL2 is required for the viability of yeast (7, 31, 32), an organism devoid of  $\beta$ -catenin. In this context, one of the salient findings of this study was that in addition to its overexpression in HCC, RUVBL2 was also found in the cytoplasm of HCC cells. This suggests that RUVBL2 serves specific cancer-related functions in the cytoplasm of tumor cells.

We have thus identified a new protein up-regulated in HCC. In vitro and in vivo results suggest that RUVBL2 could play an important role in liver carcinogenesis. Since mutations in the ATPase domains of RUVBL2 abolish its biological activity (7, 31, 32), targeting of its activity with specific inhibitors may offer a new therapeutic avenue in cancer management.

### **Acknowledgments**

We thank Marc Bonneu for proteomic analysis, Christophe Laurent for providing human liver samples, Ivan Bièche for help with primer selection for real-time PCR, and Vincent Pitard,

Nathalie Dugot-Senant and Gaëlle Cubel for their precious technical help.

## References

1. Thorgeirsson SS, Grisham JW. Molecular pathogenesis of human hepatocellular carcinoma. *Nat Genet* 2002;31:339-346.
2. Laurent-Puig P, Legoix P, Bluteau O, Belghiti J, Franco D, Binot F, Monges G, et al. Genetic alterations associated with hepatocellular carcinomas define distinct pathways of hepatocarcinogenesis. *Gastroenterology* 2001;120:1763-1773.
3. Laurent-Puig P, Zucman-Rossi J. Genetics of hepatocellular tumors. *Oncogene* 2006;25:3778-3786.
4. Takashima M, Kuramitsu Y, Yokoyama Y, Iizuka N, Toda T, Sakaida I, Okita K, et al. Proteomic profiling of heat shock protein 70 family members as biomarkers for hepatitis C virus-related hepatocellular carcinoma. *Proteomics* 2003;3:2487-2493.
5. Yokoyama Y, Kuramitsu Y, Takashima M, Iizuka N, Toda T, Terai S, Sakaida I, et al. Proteomic profiling of proteins decreased in hepatocellular carcinoma from patients infected with hepatitis C virus. *Proteomics* 2004;4:2111-2116.
6. Blanc JF, Lalanne C, Plomion C, Schmitter JM, Bathany K, Gion JM, Bioulac-Sage P, et al. Proteomic analysis of differentially expressed proteins in hepatocellular carcinoma developed in patients with chronic viral hepatitis C. *Proteomics* 2005;5:3778-3789.
7. Kanemaki M, Kurokawa Y, Matsu-ura T, Makino Y, Masani A, Okazaki K, Morishita T, et al. TIP49b, a new RuvB-like DNA helicase, is included in a complex together with another RuvB-like DNA helicase, TIP49a. *J Biol Chem* 1999;274:22437-22444.
8. Wood MA, McMahon SB, Cole MD. An ATPase/helicase complex is an essential cofactor for oncogenic transformation by c-Myc. *Mol Cell* 2000;5:321-330.

9. Bauer A, Chauvet S, Huber O, Usseglio F, Rothbacher U, Aragnol D, Kemler R, et al. Pontin52 and reptin52 function as antagonistic regulators of beta-catenin signalling activity. *Embo J* 2000;19:6121-6130.
10. Shen X, Mizuguchi G, Hamiche A, Wu C. A chromatin remodelling complex involved in transcription and DNA processing. *Nature* 2000;406:541-544.
11. Ikura T, Ogryzko VV, Grigoriev M, Groisman R, Wang J, Horikoshi M, Scully R, et al. Involvement of the TIP60 histone acetylase complex in DNA repair and apoptosis. *Cell* 2000;102:463-473.
12. Salzer U, Kubicek M, Prohaska R. Isolation, molecular characterization, and tissue-specific expression of ECP-51 and ECP-54 (TIP49), two homologous, interacting erythroid cytosolic proteins. *Biochim Biophys Acta* 1999;1446:365-370.
13. Gohshi T, Shimada M, Kawahire S, Imai N, Ichimura T, Omata S, Horigome T. Molecular cloning of mouse p47, a second group mammalian RuvB DNA helicase-like protein: homology with those from human and *Saccharomyces cerevisiae*. *J Biochem (Tokyo)* 1999;125:939-946.
14. Gorbalenya AE, Koonin EV, Donchenko AP, Blinov VM. Two related superfamilies of putative helicases involved in replication, recombination, repair and expression of DNA and RNA genomes. *Nucleic Acids Res* 1989;17:4713-4730.
15. Cho SG, Bhoumik A, Broday L, Ivanov V, Rosenstein B, Ronai Z. TIP49b, a regulator of activating transcription factor 2 response to stress and DNA damage. *Mol Cell Biol* 2001;21:8398-8413.
16. Menssen A, Hermeking H. Characterization of the c-MYC-regulated transcriptome by SAGE: identification and analysis of c-MYC target genes. *Proc Natl Acad Sci U S A* 2002;99:6274-6279.

17. Bioulac-Sage P, Rebouissou S, Sa Cunha A, Jeannot E, Lepreux S, Blanc JF, Blanche H, et al. Clinical, morphologic, and molecular features defining so-called telangiectatic focal nodular hyperplasias of the liver. *Gastroenterology* 2005;128:1211-1218.
18. Bedossa P, Poynard T. An algorithm for the grading of activity in chronic hepatitis C. The METAVIR Cooperative Study Group. *Hepatology* 1996;24:289-293.
19. Livak KJ, Schmittgen TD. Analysis of relative gene expression data using real-time quantitative PCR and the 2(-Delta Delta C(T)) Method. *Methods* 2001;25:402-408.
20. Zucman-Rossi J, Benhamouche S, Godard C, Boyault S, Grimber G, Balabaud C, Cunha AS, et al. Differential effects of inactivated Axin1 and activated beta-catenin mutations in human hepatocellular carcinomas. *Oncogene* 2007;26:774-780.
21. Halene S, Wang L, Cooper RM, Bockstoe DC, Robbins PB, Kohn DB. Improved expression in hematopoietic and lymphoid cells in mice after transplantation of bone marrow transduced with a modified retroviral vector. *Blood* 1999;94:3349-3357.
22. Richard E, Mendez M, Mazurier F, Morel C, Costet P, Xia P, Fontanellas A, et al. Gene therapy of a mouse model of protoporphyria with a self-inactivating erythroid-specific lentiviral vector without preselection. *Mol Ther* 2001;4:331-338.
23. Neaud V, Gillibert Duplantier J, Mazzocco C, Kisiel W, Rosenbaum J. Thrombin Up-regulates Tissue Factor Pathway Inhibitor-2 Synthesis through a Cyclooxygenase-2-dependent, Epidermal Growth Factor Receptor-independent Mechanism. *J Biol Chem* 2004;279:5200-5206.
24. Gerdes J, Schwab U, Lemke H, Stein H. Production of a mouse monoclonal antibody reactive with a human nuclear antigen associated with cell proliferation. *Int J Cancer* 1983;31:13-20.

25. Godichaud S, Krisa S, Couronné B, Dubuisson L, Mérillon J, Desmoulière A, Rosenbaum J. Deactivation of cultured human liver myofibroblasts by trans-resveratrol, a grapevine-derived polyphenol. *Hepatology* 2000;31:922-931.
26. Nicoletti I, Migliorati G, Pagliacci MC, Grignani F, Riccardi C. A rapid and simple method for measuring thymocyte apoptosis by propidium iodide staining and flow cytometry. *J Immunol Methods* 1991;139:271-279.
27. Griffiths GJ, Dubrez L, Morgan CP, Jones NA, Whitehouse J, Corfe BM, Dive C, et al. Cell damage-induced conformational changes of the pro-apoptotic protein Bak in vivo precede the onset of apoptosis. *J Cell Biol* 1999;144:903-914.
28. Mandic A, Viktorsson K, Molin M, Akusjarvi G, Eguchi H, Hayashi SI, Toi M, et al. Cisplatin induces the proapoptotic conformation of Bak in a deltaMEKK1-dependent manner. *Mol Cell Biol* 2001;21:3684-3691.
29. Colucci F, Soudais C, Rosmaraki E, Vanes L, Tybulewicz VL, Di Santo JP. Dissecting NK cell development using a novel alymphoid mouse model: investigating the role of the c-abl proto-oncogene in murine NK cell differentiation. *J Immunol* 1999;162:2761-2765.
30. Obeid LM, Linardic CM, Karolak LA, Hannun YA. Programmed cell death induced by ceramide. *Science* 1993;259:1769-1771.
31. Jonsson ZO, Dhar SK, Narlikar GJ, Auty R, Wagle N, Pellman D, Pratt RE, et al. Rvb1p and Rvb2p are essential components of a chromatin remodeling complex that regulates transcription of over 5% of yeast genes. *J Biol Chem* 2001;276:16279-16288.
32. Lim CR, Kimata Y, Ohdate H, Kokubo T, Kikuchi N, Horigome T, Kohno K. The *Saccharomyces cerevisiae* RuvB-like protein, Tih2p, is required for cell cycle progression and RNA polymerase II-directed transcription. *J Biol Chem* 2000;275:22409-22417.

33. Willis SN, Chen L, Dewson G, Wei A, Naik E, Fletcher JI, Adams JM, et al. Proapoptotic Bak is sequestered by Mcl-1 and Bcl-xL, but not Bcl-2, until displaced by BH3-only proteins. *Genes Dev* 2005;19:1294-1305.
34. Eskes R, Desagher S, Antonsson B, Martinou JC. Bid induces the oligomerization and insertion of Bax into the outer mitochondrial membrane. *Mol Cell Biol* 2000;20:929-935.
35. Wei MC, Lindsten T, Mootha VK, Weiler S, Gross A, Ashiya M, Thompson CB, et al. tBID, a membrane-targeted death ligand, oligomerizes BAK to release cytochrome c. *Genes Dev* 2000;14:2060-2071.
36. Kim JH, Kim B, Cai L, Choi HJ, Ohgi KA, Tran C, Chen C, et al. Transcriptional regulation of a metastasis suppressor gene by Tip60 and beta-catenin complexes. *Nature* 2005;434:921-926.
37. Guo XZ, Friess H, Di Mola FF, Heinicke JM, Abou-Shady M, Graber HU, Baer HU, et al. KAI1, a new metastasis suppressor gene, is reduced in metastatic hepatocellular carcinoma. *Hepatology* 1998;28:1481-1488.



## Figure legends

### Figure 1 : RUVBL2 expression in hepatocellular carcinoma

A : Zoom on an area of 2-dimensional gels showing a spot more abundant in tumoral (T) than non-tumoral (NT) tissue. Note that other spots in the area are of similar intensity in both samples.

B : Western blot of RUVBL2 expression in the 4 samples of HCC and paired non tumoral liver used for proteomic analysis. The blot was subsequently rehybridized with a  $\beta$ -actin antibody.

### Figure 2 : Immunohistochemical detection of RUVBL2 in liver samples

A : Immunostaining of RUVBL2 in a normal liver at distance of an hemangioma. Hepatocytes nuclei are irregularly and mildly stained; in addition biliary cells of an interlobular bile duct in a portal tract show a strong nuclear and cytoplasmic staining (arrow). Inset : higher magnification from another normal liver showing the heterogeneous nuclear staining as well as the intense bile duct cells staining.

B : A serial section incubated with a non immune IgG shows no staining.

C : Immunostaining of HCC and surrounding cirrhotic liver (Cir) demonstrates the overexpression of RUVBL2 in HCC and shows that the staining of tumoral hepatocytes is heterogeneous, from mild to strong

D : High magnification of a zone from the HCC shown in 2C illustrates a strong staining of cytoplasm

E : High magnification of another HCC case with less intense although definite cytoplasmic staining

F : In surrounding cirrhotic nodules, hepatocytes show only a nuclear staining. Biliary cells of the ductular reaction (arrows) are intensely stained. Some lymphocytes in the fibrous tissue are also stained (arrowhead).

### **Figure 3 : Correlations between RUVBL2 mRNA levels and clinico-pathological features of HCC**

RUVBL2 mRNA level was measured by RT-QPCR. Gene expression results were first normalized to internal control ribosomal 18S in all samples. Then, results in HCC samples were expressed as a ratio relatively to the mean expression level in a pool of 15 non-tumor samples.

A : differences between non-tumor and tumor samples in the series of 96 HCCs

B : RUVBL2 expression according to HBV status (HBV infected, n = 9; non infected, n = 78)

C : RUVBL2 expression according to tumor grade (grade I, n = 3; grade II, n= 37; grade III, n= 47, grade IV, n= 6)

D : RUVBL2 expression in relation to the presence of  $\beta$ -catenin mutations

### **Figure 4 : Knock-down of RUVBL2 expression leads to reduced proliferation and cell death**

A : Western blot of RUVBL2 expression. HuH7 cells were transfected with siRNA duplexes at Day 0. At indicated times, cells were lysed and processed for Western blot with anti-RUVBL2 and anti- $\beta$ -actin antibodies.

B : Cell proliferation was measured with a Coulter counter at indicated times post-transfection of siRNA duplexes. Shown are the mean  $\pm$  SEM of 3 experiments conducted in duplicate. Symbols are as follows : lozenges (non transfected), triangles (scrambled), open squares

(siR1), closed squares (siR2). The growth of siR1 and siR2 transduced cells was significantly reduced as compared to controls ( $p < 0.001$  by ANOVA).

**C- At Day 4 post-transfection, cells were labeled with Ki67 antibody and the percentage of labeled cells was measured with flow cytometry. NT = non transfected. The percentage of labeled cells was significantly reduced with siR1 and siR2 as compared to both controls ( $p < 0.002$  by ANOVA).**

D-I : At Day 6 post-transfection of scrambled siRNA (D, F, H) or RUVBL2 siRNA (siR1, E, G, I), cells were simultaneously stained with DAPI (D, E) and antibody to activated caspase-3 (F, G). Arrows indicate cells with fragmented nuclei and cytoplasmic staining for activated caspase-3. H and I are merged pictures.

J : At Day 6 post-transfection, the percentage of cells with fragmented DNA was measured by flow cytometry following propidium iodide staining. Results are expressed relatively to the values found in scrambled-transfected cells and are the mean  $\pm$  SD of 3 experiments in duplicate. White bar : control ; grey bar : siR1 ; black bar : siR2. DNA fragmentation was significantly increased in siR1 and siR2 transduced cells as compared to controls ( $p < 0.001$  by ANOVA).

K : At Day 6 post-transfection, caspase 3 activity was measured with a colorimetric substrate. Results are expressed relatively to the values found in scrambled-transfected cells and are the mean  $\pm$  SD of 3 experiments in duplicate. White bar : control ; grey bar : siR1 ; black bar : siR2. Caspase-3 activity was significantly increased in siR1 and siR2 transduced cells as compared to controls ( $p < 0.005$  by ANOVA).

### **Figure 5 : RUVBL2 downregulation induces pro-apoptotic gene expression**

**A : At 5 days following siRNA transfection, cells were analyzed by flow cytometry with conformation-sensitive Bak-1 (left panel) of Bax (right panel) antibodies. Gray peaks indicate**

scramble-transfected cells, black line, siR1-transfected cells. Non-transfected cells are not shown for clarity but showed identical results as scramble-transfected cells.

B : Quantification of 3 independent transfection experiments. One-way analysis of variance showed that results differed overall significantly between groups ( $p = 0.0002$  for Bak-1,  $p = 0.006$  for Bax). Significant differences between individual groups were assessed with the post-hoc Tukey's test and are shown on the graphs.

C, D : Cells were transfected with siRNAs as in Fig. 4. Total RNA was extracted at Days 3 (C) and 4 (D), and gene expression was measured using real time RT-PCR. Results were normalized on the basis of the expression of the RLP0 gene and on the levels of the non transfected samples. Black bars indicate non transfected cells, white bars, scramble-transfected cells, and striped bars, cells transfected with siR1. The graph shows the mean  $\pm$  SD of 3 independent experiments. Numbers indicate the p value using ANOVA.

**Figure 6 : Up-regulation of RUVBL2 expression enhances anchorage-independent growth, protects against apoptosis, and leads to more rapidly progressive tumors in vivo**

A: Cell lysates from cells transduced with the control lentivirus (lane 1) or the Flag-RUVBL2 vector (lane 2) were examined by Western blot with an anti-RUVBL2 antibody. The blot was rehybridized with an antibody to  $\beta$ -actin.

B : Control (black bar) or Flag-RUVBL2-expressing cells (open bar) were seeded in soft agar at clonal density. The surface area of colonies was measured after 2 weeks. Results are expressed relatively to the values found in control cells and are the mean  $\pm$  SD of 3 experiments in triplicate.

C : Control (closed squares) or Flag-RUVBL2-expressing cells (open squares) were incubated with the indicated concentrations of C2 ceramide for 15-17h. Cell viability was assessed with the MTT assay. Results are expressed as the percentage of viability as compared to untreated

cells, and are shown as mean  $\pm$  SEM of 5 experiments in triplicate. One-way analysis of variance showed that results differed overall significantly between groups ( $p < 0.001$ ). Significant differences between individual groups were assessed with the post-hoc Tukey's test (\* :  $p < 0.05$ ; #  $p < 0.001$ ).

D : Control (black bars) or Flag-RUVBL2 expressing cells were incubated with the indicated concentrations of C2 ceramide for 17h and the percentage of cells with fragmented DNA was measured by flow cytometry following propidium iodide staining. Results are the mean  $\pm$  SEM of 3 experiments. One-way analysis of variance showed that results differed overall significantly between groups ( $p < 0.001$ ). Asterisks indicate significant differences between individual groups by the post-hoc Tukey's test ( $p < 0.01$ ).

E : Control (closed squares) or Flag-RUVBL2-expressing cells (open squares) were injected subcutaneously to immunocompromised mice (20 mice per group). Tumor growth was monitored periodically. Results are expressed as mean tumor volume  $\pm$  SEM. The 2 groups differed significantly by ANOVA.

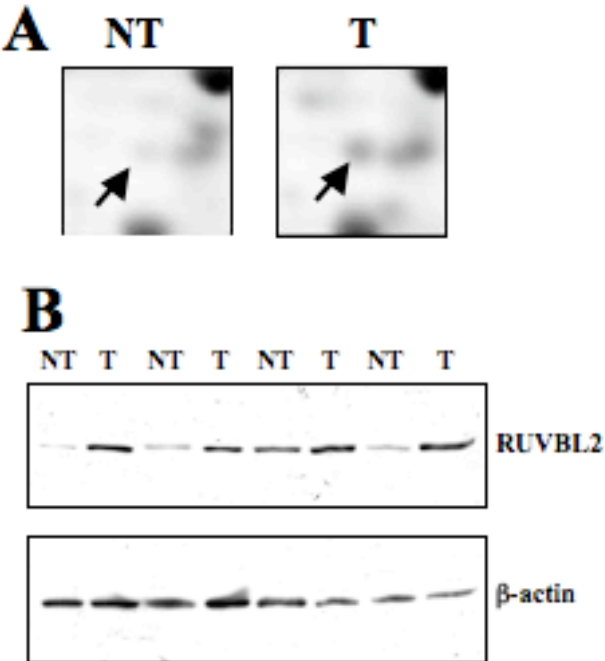
F : A subset of tumors were analyzed at the end of the experiment by Western blot with antibodies to RUVBL2 (upper panel), Flag (middle panel) or  $\beta$ -actin (lower panel).

**Table 1. Characteristics of patients and tumors (n=96)**

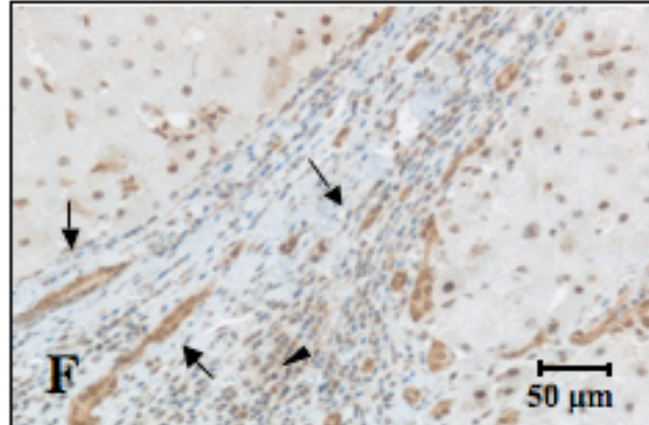
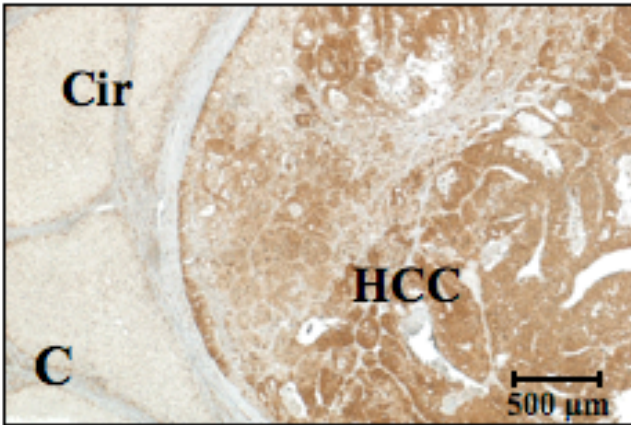
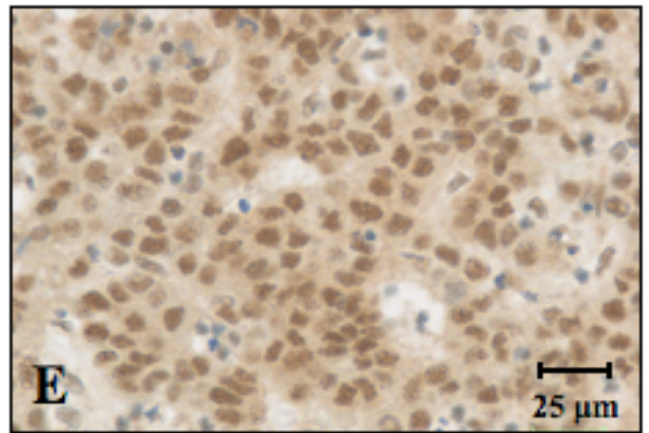
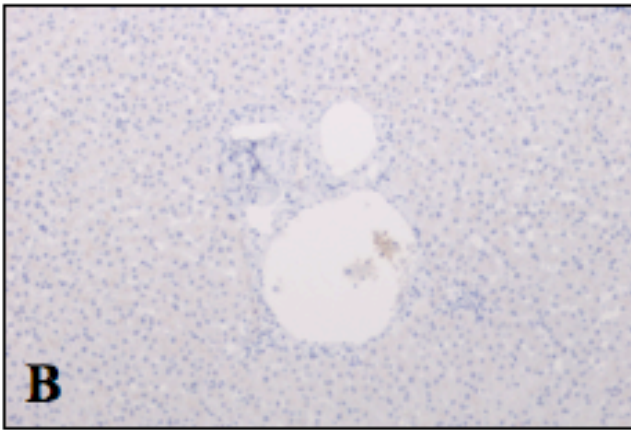
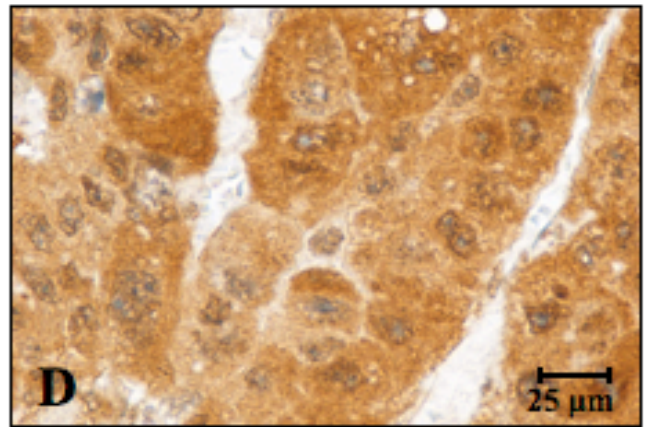
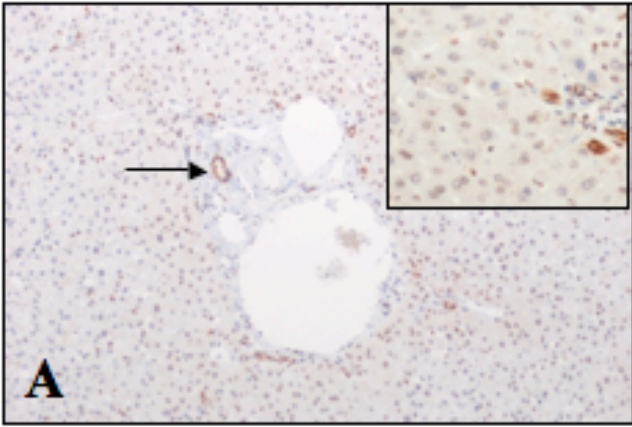
<b>Clinical characteristics</b>	
Age (mean $\pm$ SD)	64.6 $\pm$ 10.6 years
Gender (male)	87.5%
AFP < 20 ng/ml	63%
Cirrhosis or chronic active hepatitis	60%
HBV infection	10%
HCV infection	25%
Alcohol	55%
Hemochromatosis	3%
<b>Tumors characteristics</b>	
Diameter (mean $\pm$ SD )	7.1 $\pm$ 5 cm
Intact capsule	16%
Satellite nodule	41%
Edmondson grade III or IV	57%
Microscopic vascular embolus	36%
<i>CTNNB1</i> mutations	35%

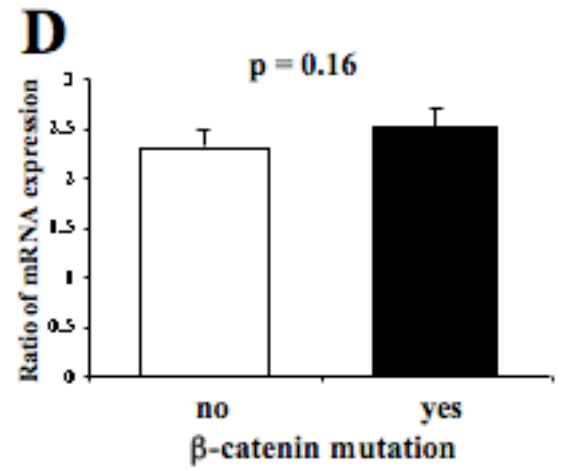
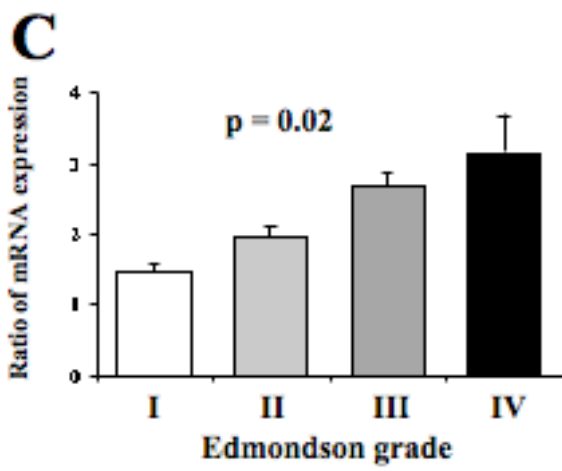
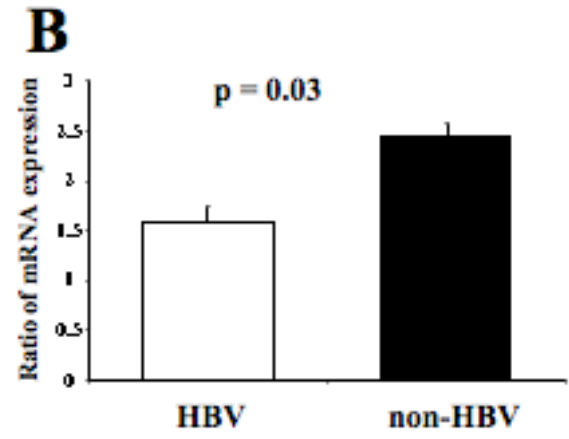
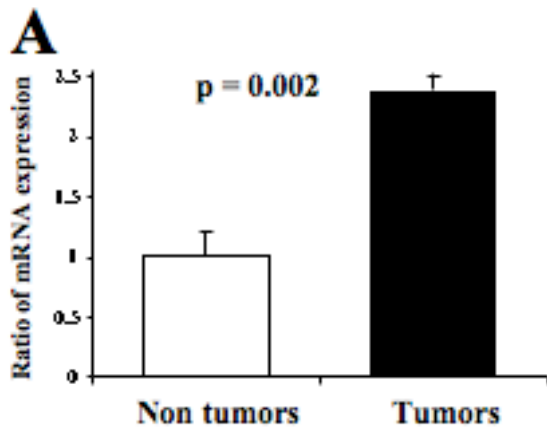
**Supplementary Table 1. Sequences of primers used for PCR**

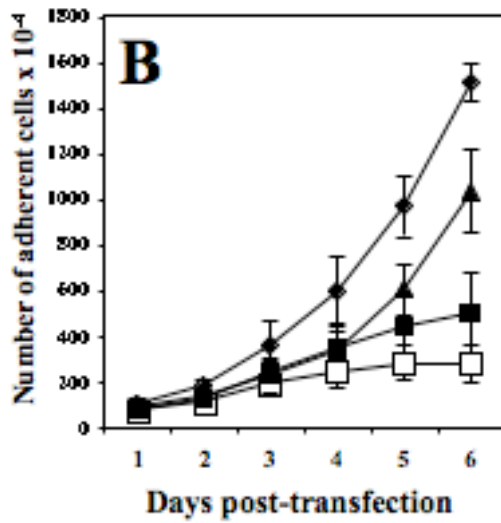
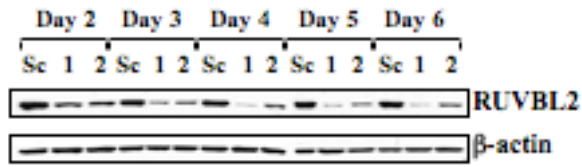
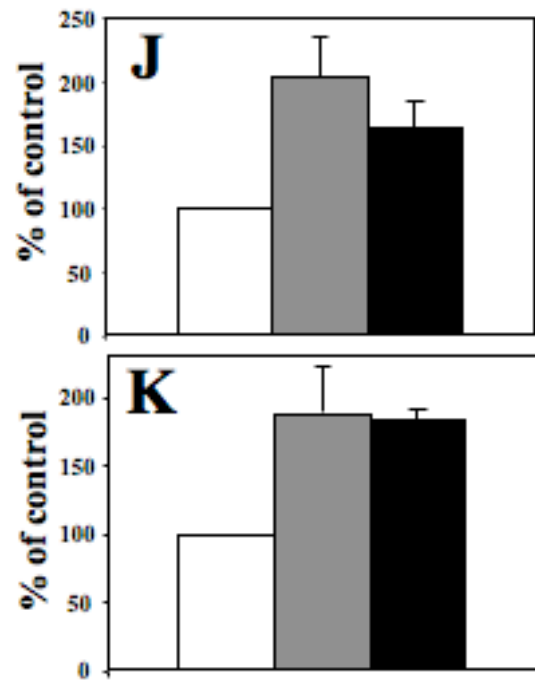
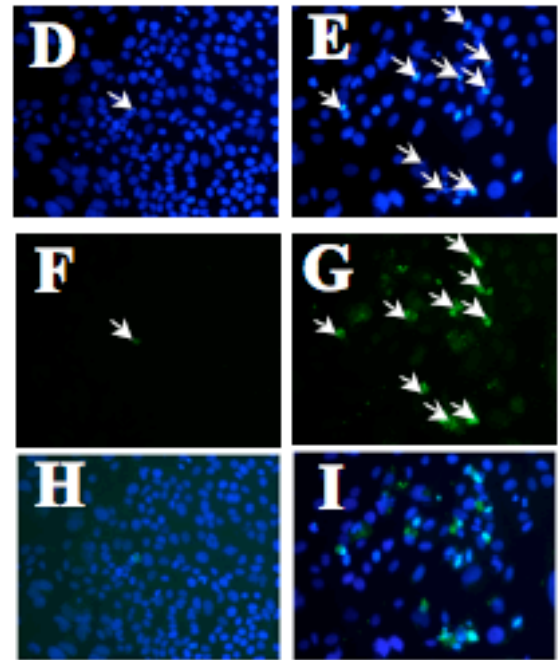
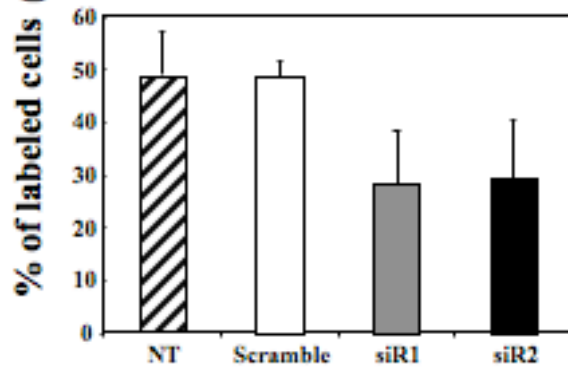
<b>Gene</b>	<b>Primers sequence</b>
<b>BAD</b>	U : 5' CCC AAC CTC TGG GCA GCA C 3' L : 5' CGA GGA AGT CCC TTC TTA AAG GAG T 3'
<b>BAK-1</b>	U : 5' CAA GAT TGC CAC CAG CCT GTT 3' L : 5' AGG CCA TGC TGG TAG ACG TGT A 3'
<b>BAX</b>	U : 5' GTG CCT CAG GAT GCG TCC A 3' L : 5' ACG GCG GCA ATC ATC CTC T 3'
<b>PUMA</b>	U : 5' AGTACGAGC GGC GGA GAC A 3' L : 5' GGA GTC CCA TGA TGA GAT TGT ACA G 3'
<b>BCL-xS</b>	U : 5' GAC ATC CCA GCT CCA CAT CAC 3' L : 5' GTT CCA CAA AAG TAT CCT GTT CAA A 3'
<b>BCL-xL</b>	U : 5' TGA ATG ACC ACC TAG AGC CTT GGA 3' L : 5' GGA ACC AGC GGT TGA AGC GT 3'
<b>BID</b>	U : 5' CGT CCT TGC TCC GTG ATG TCT T 3' L : 5' TCC GTT CAG TCC ATC CCA TTT C 3'
<b>RLP0</b>	U : 5' GGC GAC CTG GAA GTC CAA CT 3' L : 5' CCA TCA GCA CCA CAG CCT TC 3'

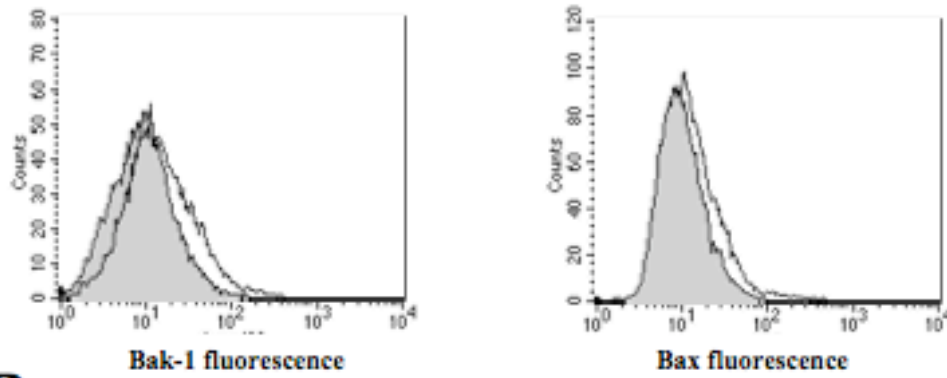
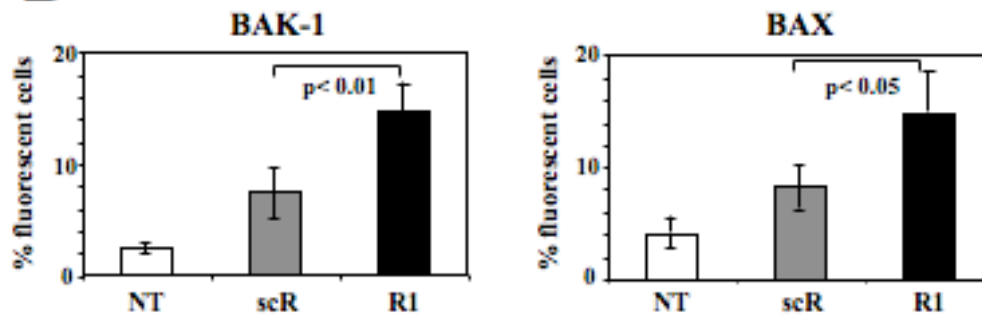
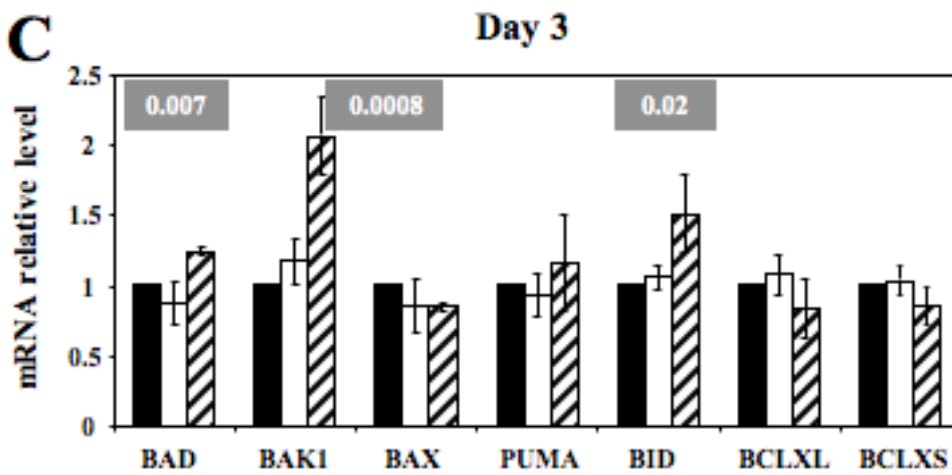








**A****C**

**A****B****C****D**